

Quantum Key Distribution Using an Integrated Quantum Emitter in Hexagonal Boron Nitride

Ali Al-Juboori,^{1, 2, *} Helen Zhi Jie Zeng,^{1, *} Minh Anh Phan Nguyen,¹ Xiaoyu Ai,² Arne Laucht,^{2, †} Alexander Solntsev,¹ Milos Toth,^{1, 3} Robert Malaney,² and Igor Aharonovich^{1, 3, ‡}

¹*School of Mathematical and Physical Sciences, Faculty of Science, University of Technology Sydney, Ultimo, New South Wales, 2007, Australia*

²*School of Electrical Engineering and Telecommunications, The University of New South Wales, Sydney, NSW 2052, Australia*

³*ARC Centre of Excellence for Transformative Meta-Optical Systems, Faculty of Science, University of Technology Sydney, Ultimo, New South Wales, 2007, Australia*

Quantum Key Distribution (QKD) is considered the most immediate application to be widely implemented amongst a variety of potential quantum technologies. QKD enables sharing secret keys between distant users, using photons as information carriers. The current challenge is to implement these protocols in practice, for real-world conditions, in a robust, and compact manner. Single Photon Sources (SPS) in solid-state materials are prime candidates in this respect. Here, we demonstrate a room temperature, discrete-variable quantum key distribution system using a bright single photon source in hexagonal-boron nitride, operating in free-space. Employing an integrated, “plug and play” photon source system, we have generated keys with one million bits length, and demonstrated a secret key of approximately 70,000 bits, at a quantum bit error rate of 6%, with ϵ -security of 10^{-10} . Emphasis was put on the inclusion of all known effects impacting the derived security level, thereby demonstrating the most trustworthy QKD system realised with SPSs to date. Our results will be important to achieve meaningful progress with deterministic room-temperature QKD systems.

I. INTRODUCTION

Secure and hacking-proof communications is a vital requirement in today’s world. Traditional public key cryptography relies on lengthy and hard to decipher mathematical functions to encrypt and decrypt data. However, with the advancements of quantum computers, secured communication is increasingly vulnerable to hacking attempts. Quantum Key Distribution (QKD) [1–3] the best-known application of quantum cryptography, offers an information-theoretic secure communication system, largely on account of the quantum non-cloning theorem [4]. It enables two users to generate the exact same key without sharing any part of it publicly, providing a solution to secure key exchange. Since its inception in mid-1980s, and the first successful proof-of-concept test [5], QKD has evolved to include various approaches such as entanglement-based QKD [6–8], measurement-device-independent QKD [9], quantum teleportation-based QKD [10], and satellite-based QKD [11]. So far the majority of QKD systems rely on either nonlinear down-converted sources or attenuated lasers [12, 13]. The advantage of these latter sources is their potentially high repetition rate. However, the issue remains that these sources are probabilistic, and remain unsecured even with proper counter measures in place, such as the decoy protocol [14]. One alternative approach is using a deterministic, triggered single photon source (SPS) that emits a single

photon per excitation cycle. Over the last few decades, significant effort has been put forward to develop such sources, with prime challenges being their purity (i.e., minimisation of multiphoton events) and extraction of light (i.e., collection efficiencies) [15, 16]. While semiconductor quantum dots are a great choice for a bright and pure source [6, 17, 18], their operation is limited to cryogenic temperatures. For wide deployment and practical implementation of QKD in real-world settings, compact, room temperature, sources are required [19–22].

Among the various solid-state materials, single-photon sources in hexagonal boron nitride (hBN) are considered a prime candidate for QKD owing to the material’s favourable physical and optical properties [23]. In particular, properties such as a high single-photon purity, and high-brightness operating in ambient conditions give a competitive advantage over other sources [24].

After having demonstrated the in-principle usability of hBN SPSs for QKD in Ref. 24, in this work, we include a full implementation of a free-space, discrete-level QKD system using an integrated SPS in hBN. We implement the BB84 protocol, demonstrating the sending, receiving and encryption/decryption process of an image from one device to another. We perform all security protocols, including privacy amplification, to demonstrate the most reliable QKD realised with SPSs to date.

II. SETUP CONFIGURATION

The optical apparatus used to perform the measurements as a whole can be split into two main systems; the source to generate the single photons, and the QKD apparatus to perform the key distribution measurements.

* These authors contributed equally to this work.

† a.laucht@unsw.edu.au

‡ Igor.Aharonovich@uts.edu.au

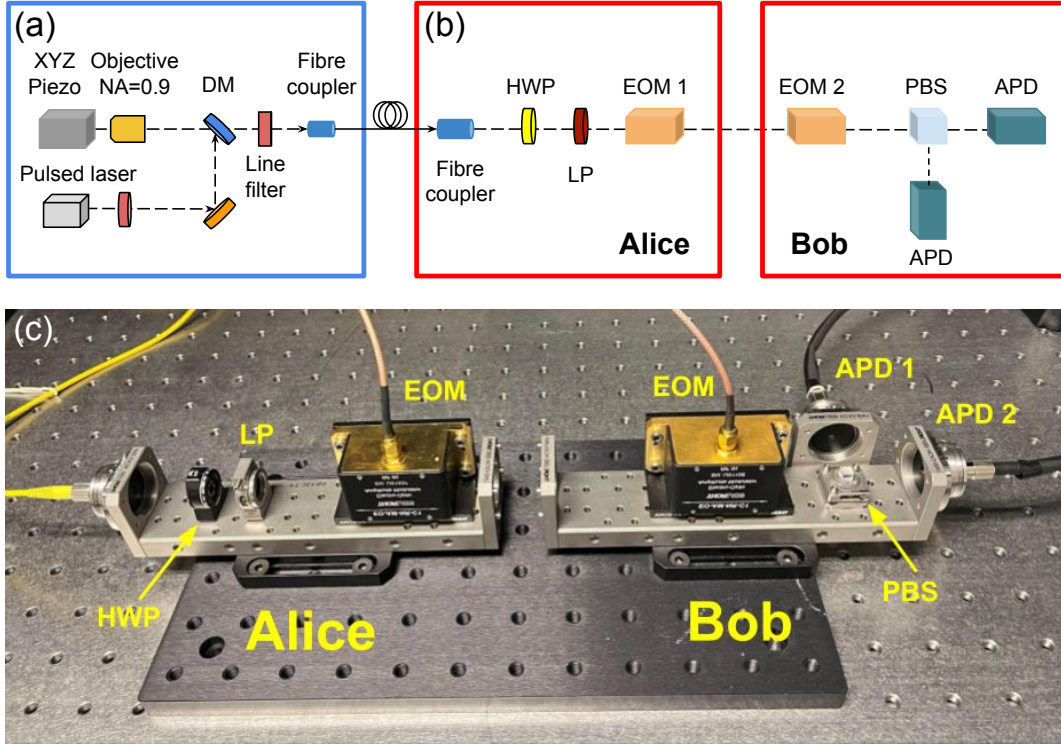


Figure 1 (a) Schematic diagram of the single-photon source. DM, dichroic mirror. (b) Schematic diagram of the QKD setup. EOM, electro-optic modulator; LP, linear polariser; APD, avalanche photodiode; PBS, polarising beam splitter; HWP, half-wave plate. (c) The optical components of the transmitter (Alice) and the receiver (Bob).

The hBN single photon sources are the primary source of photons for the QKD system. The sources are integrated with a solid immersion lens and packaged into a compact, portable device as described previously [24] and shown schematically in Figure 1a. For the QKD experiments, the sources are excited using a 515 nm pulsed laser (PicoQuant PDL-800D), and the collection is coupled via single mode optical fibre to the QKD sender (Alice).

The QKD-side setup is shown in Figure 1b. The management and distribution of keys are performed by elements which modulate and/or measure the polarisation of the photons. The elements lie in a transmitter and receiver, termed Alice and Bob, respectively, that are separated by tens of centimetres in free space. The signal from the source is sent to the Alice, firstly. Alice consists of a half-wave plate (FBR-AH1, Thorlabs), linear polariser (FBRP, Thorlabs), and an electro-optic modulator (EOM) (EO-AM-NR-C1, Thorlabs). The half-wave plate and linear polariser are used to align and filter vertically polarised photons, respectively, minimising losses as they enter the EOM – a requirement for its function. The EOM is driven by a digital-to-analogue converter (DAC) (EVAL-AD5754REBZ, Analog Devices), multiplexer (MUX36D04EVM-PDK, Texas Instruments), and a high voltage amplifier (HVA 200, Thorlabs), supplying the four voltages (two voltages in Bob's case) to the EOMs to induce the desired polarisation states. Bob consists of

an EOM, polarising beam splitter (PBS052, Thorlabs), and two avalanche photodiodes (APD, SPCMAQRH-12-FC, Excelitas).

III. EXPERIMENTAL PROCEDURE AND RESULTS

We start by choosing the most appropriate hBN SPSs – in particular, those with a high single-photon purity. Figure 2a shows the spectrum of the hBN SPS used in all QKD runs reported here. This SPS has a characteristic sharp zero-photon line (ZPL) at 645 nm. The emission was then bandpass filtered (Semrock, 650 ± 13 nm) to select only photons from around the ZPL for the QKD experiment. The bandpass filtering was crucial in overcoming the wavelength dependence of the EOM and ensuring that the single-photon purity remains as low as possible, with Figure 2b showing the second-order autocorrelation function $g^{(2)}(0) = 0.08$. Additionally, the count rate was measured as a function of pulsed excitation power at a pulse repetition rate of 40 MHz, as shown in Figure 2c. The SPS was found to saturate at an average pulsed-excitation power of $217 \mu\text{W}$ with a count rate of $5.08 \times 10^5 \text{ cts/s}$ as out-coupled from the single-mode fibre. From this, the calculation of the source-side total setup efficiency can be quantified with a mean photon

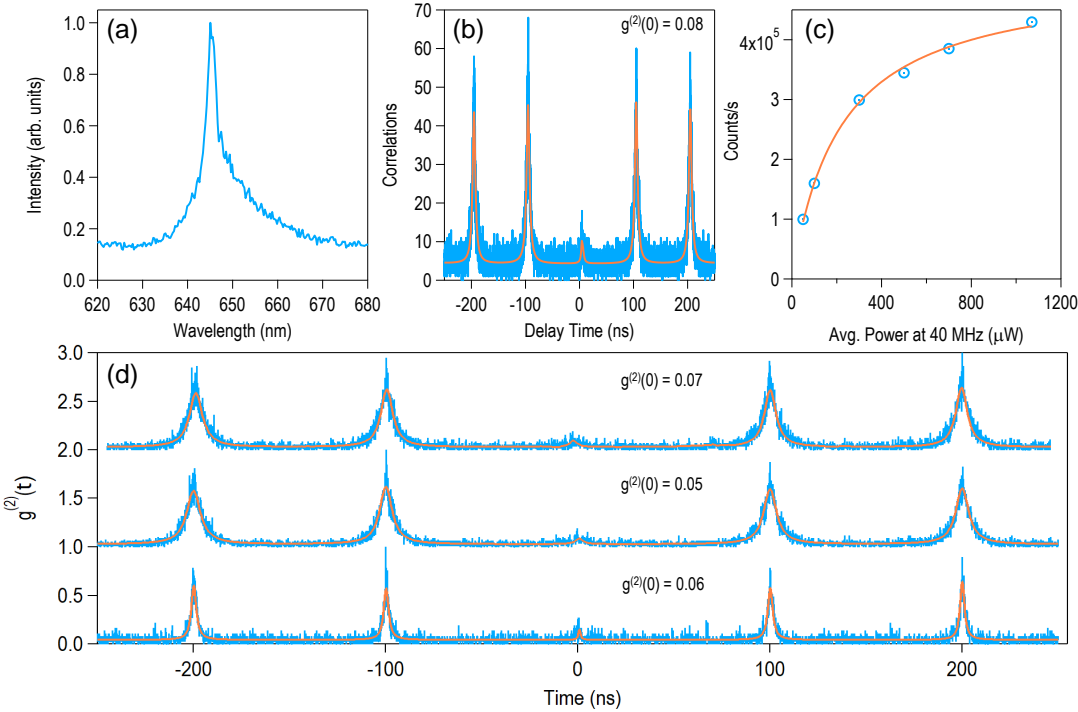


Figure 2 Optical characteristics of the hBN SPS as measured through the SIL. (a) Spectrum of the SPS used for QKD, showing a sharp ZPL at 645 nm. (b) Pulsed second-order autocorrelation function of the QKD SPS at 10 MHz, showing a $g^{(2)}(0) = 0.08$. (c) Power-dependent saturation measurements showing count rate as a function of pulsed excitation power at 40 MHz repetition rate. (d) Pulsed second-order autocorrelation measurements of three characteristic SIL-integrated hBN SPSs, showing typical single-photon purity. All measurements were performed at 10 MHz repetition rate.

number per pulse of $\mu = 0.012$. This can be substantially improved by optimising the collection further, employing different designs [25, 26]. Importantly, our modular design enables rapid characterisation and swapping of other sources. Examples of three other suitable sources with low $g^{(2)}(0)$ values are shown in Figure 2d.

Having characterised and established the source of single photons, the testbed for the QKD system was then initiated. Figure 3 shows the operation sequence of the QKD process. The process starts with Alice generating a sequence of random integer numbers, each of which is 0, 1, 2 or 3, while Bob generates a sequence of random numbers between 0 and 1. Alice's numbers are used to encode the measurement bases and bit values onto the photons, while Bob's numbers are used to select the measurement bases for the measurements.

More specifically, Alice's numbers map to one of four polarisation states imparted to the photons, horizontal (H, \leftrightarrow), vertical ($V, \uparrow\downarrow$), right-handed circular (R, \circlearrowright), or left-handed circular (L, \circlearrowleft). For each laser pulse cycle, at a rate of 500 kHz, Alice's randomly generated number switches a multiplexer to select a specific one of four channels from the digital-to-analogue converter (DAC) to apply a predetermined voltage to the EOM and, as such, encodes the desired polarisation state onto the photon.

Bob uses a corresponding setup to randomly select a basis, H/V or R/L , and measure the photon to obtain one

of four outcomes. Bob's EOM either leaves the incoming photon in its polarisation base or interchanges linear and circular polarisation. The PBS (polarising beam splitter) then separates linearly polarised photons with certainty to be detected at one of two detectors, whereas circularly polarised photons are unpredictably registered at either one of the two detectors. Bob's APDs are gated to the laser pulse, and only the detection event of a single photon by one of the APDs per time bin is considered a valid bit and stored to the computer, while the rest is discarded.

After revealing their bases used, Alice and Bob “sift” their events, discarding those which have mismatched bases. By defining H and R to correspond to a bit value of “0”, and V and L to correspond to a bit value of “1”, respectively, Alice and Bob retain a partially-correlated string of random bits. This string must be processed further to obtain a *secret key*.

The required number of bits in the partially-correlated string must be large enough to provide a non-zero secret key rate at the pre-assigned ε -security (total failure probability), as discussed in the appendix. After accumulating the required number of bits, the post-processing procedure is initiated, a first component of which is parameter estimation. After this, a next phase is commenced, which consists of reconciliation and privacy amplification, after which the final secret key is generated.

In the QKD experiments we transmitted blocks of 1

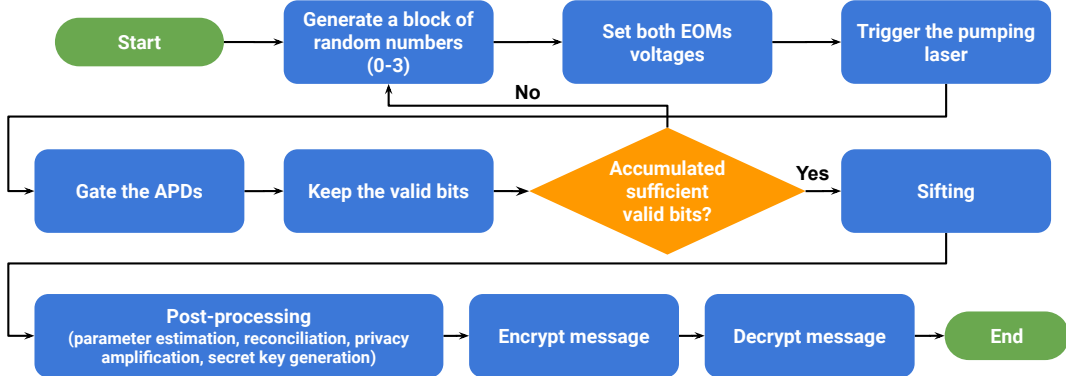


Figure 3 QKD operation sequence.

Experiment no.	1	2	3	4	5	6
Clock rate (kHz)	500,000	500,000	500,000	500,000	500,000	500,000
Photon detection rate at Bob (cts/s)	1527	1486	1375	1722	1666	1001
Raw key length (bits)	1,000,000	1,000,000	100,000	100,000	10,000	10,000
Raw key rate (bits/s)	88	96	80	100	96	56
Bounded raw key rate (bits/s)	396	432	360	450	432	252
QBER	0.07	0.06	0.08	0.05	0.03	0.08

Table I Selected experimental runs with their respective parameters.

million random bits at a clock rate of 500 kHz (limited by the voltage amplifier and the EOM), resulting in a 2 s transmission phase during which Bob received photons at a detection rate of ≈ 1500 cts/s. After this transmission phase, our system required 7 s for the data processing phase (dominated by the data transfer between the FPGA board and the PC), resulting in a total of 9 s per block of 1 million random bits. During the experiments no. 1 and no. 2 (in Table I) we repeated the transmission of these blocks until 4 million valid bits were accumulated (see also flow chart in Figure 3). 50% of the accumulated bits are sacrificed during the sifting process, while another 50% of the remaining bits are used for the quantum bit error rate (QBER) estimation. The partially-correlated keys that exist at this phase are referred to as the ‘*raw keys*’. Error correction is then instigated to turn the partially-correlated pair of keys into identical keys. Following this, the now correlated keys are input to the privacy amplification process of which, approximately 1/16th end up as the final secret keys (see appendix for details on error correction and privacy amplification).

We repeated the QKD measurement numerous times, accumulating raw keys of lengths up to 10^6 bits (after sifting and QBER estimation). Representative results for several independent runs of different lengths are shown in Table I, with QBER values ranging between 3% and 8%.

Our experimental set up was primarily aimed at the development of the most reliable key in terms of ε -security, not the key rate. Hardware limitations imposed certain constraints on us, related to the amount of quantum information that could be transferred before classical pro-

tocols were implemented (e.g., TCP socket connections, memory-read functions), which led to time delays of 7 s per million bit-transfer attempts. Of course, such processing delays can never be set to zero in any implementation, but if we simply set all such delays to zero, we derive what we refer to as the *bounded raw key* rate in Table I. Beyond the time delays, the three most important factors influencing the raw key rate are (i) the input pump rate; (ii) capture rates from the photon source; and (iii) losses in our optical components. Achievable improvements in these three factors alone would readily lead us into the ~ 10 kHz raw key rate range.

For runs no. 1 and no. 2 (in Table I) we also performed privacy amplification at ε -security levels of 10^{-10} and below, and achieved secret key lengths of 33176 bits & 68516 bits at secret key rates of 4 (bits/s) & 6 (bits/s) or bounded secret key rates of 18 (bits/s) & 26 (bits/s), respectively. For the other runs in Table I, finite key effects result in zero secret key rates at a ε -security level of 10^{-10} .

Finally, to demonstrate the QKD utility, we transfer an image in a secured way from Alice to Bob. The image of a toy car consisting of 48 kbytes is shown in Figure 4a. We use the key from the QKD experiment no. 2 (see Table I) as a one-time keypad to encrypt the image (Figure 4b). Alice then transmits the image to Bob classically, and Bob decrypts the image using the secure key at his end, as shown in Figure 4c.

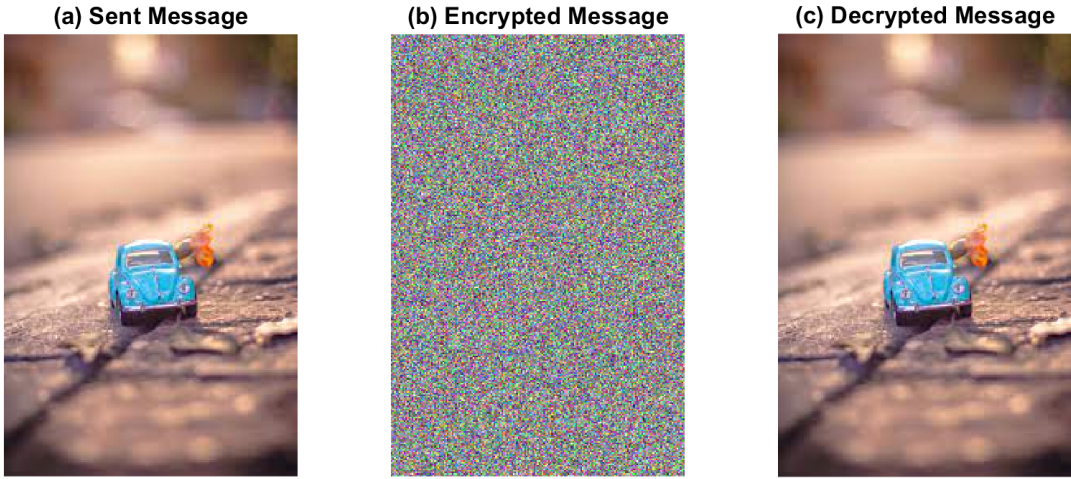


Figure 4 (a), Original image, (b) image encrypted with Alice’s secure key, and (c) the decrypted image after decoding it using Bob’s secure key.

IV. DISCUSSION AND OUTLOOK

We report a functional, free-space, room-temperature QKD prototype with high-purity hBN SPSs. We implement a complete BB84 protocol, including privacy amplification and QBER corrections at a security level (total failure probability) of 10^{-10} . As discussed further in the appendix, although our rates are lower relative to others seen in the literature [20, 27, 28], straightforward comparison of the many published results should be done with caution as many different assumptions and security settings can be in place. In addition, our clock rate operates at 500 kHz, compared to other experiments that trigger at a few MHz rates, or faster.

Furthermore, we have included all possible assumptions in our derivation of security in the finite key limit, including the possibility of vacuum contributions affecting the probability of multiple photon events [29, 30]. We believe our experimental secret key rates currently represent the most reliable in terms of security for the type of photon source used. Increasing the rate at a given security level, can be achieved via various improvements in the system – including an increased photon collection rate from the SPS, increased speed in the electronics, and increased computational power for the classical reconciliation. For instance, one key limitation originates from the high voltage amplifiers needed to drive the EOMs, which can be improved using alternative hardware. Using different field-programmable gate array (FPGA) hardware and data transfer protocols, can also further increase the rates.

All in all, our source has one of the best purities at room temperature, with an excellent brightness, and operation under ambient conditions that can enable a straightforward integration with existing QKD networks. Our work paves the way for scalable implementation of QKD systems and holds great promise for using triggered

room temperature SPSs based on hBN.

ACKNOWLEDGEMENTS

The authors thank Timm Kupko, Tobias Heindel, Oliver Benson, Esteban Gómez-López, Çağlar Samaner, Serkan Ateş, and Francois Ladouceur for useful discussions. We also thank Rich Mildren and Adam Bennett for the initial assistance of the source integration. This work is supported by the Australian Research Council (CE200100010), and the Office of Naval Research Global (N62909-22-1-2028). We thank the NSW Defence Innovation Network, the NSW State Government, and the Next Generation Technologies Fund for financial support of this project funded by the DIN Strategic Investment Initiative.

Appendix A: Reconciliation

Reconciliation is a classical post-processing step that corrects the discrepancies between Alice and Bob's bit strings. Let us assume the estimated QBER, Q , is already achieved (via the prior sacrifice of m bits) and that Alice and Bob start reconciliation with two bit strings (the raw keys), K_A and K_B , each of length n bits. The common treatment is to break K_A and K_B into shorter sub-blocks and then reconcile them in parallel [31]. Applying this treatment to our experiments, the procedure of reconciliation is as follows:

- **Step 1: Partition.** Alice breaks her K_A into multiple sub-blocks and the size of each sub-block is set to n_{block} ($n_{\text{block}} \leq n$). Bob does the same to his K_B . Then, Alice and Bob will apply Step 2 and 3 to each of their sub-blocks. In our experiments we set $n_{\text{block}} = 10^4$, and note that a maximum of 8 sub-blocks can be simultaneously reconciled due to the limited number of threads available at Alice.
- **Step 2: Syndrome Calculation.** Bob applies an LDPC matrix, \mathbf{H} , to his sub-block and obtains syndrome bits. Then, Bob sends the syndrome bits, S_B (of length s_B), to Alice via classical communications. We adopted an LDPC code designed to maximise its decoding threshold at a code rate, $R_c = 0.5$. [Note, the decoding threshold of a given LDPC code is the maximal bit error rate so that a belief-propagation decoder is guaranteed to correct all the errors in an LDPC block [32] - it can be maximised by using *Density Evolution* [32].] The degree distribution polynomials of the adopted code can be found in Table I of [33]. The matrix \mathbf{H} (with $n_{\text{block}}(1 - R_c)$ rows and n_{block} columns) was constructed by the Progressive Edge Growth (PEG) algorithm [34] based on the above mentioned polynomials.
- **Step 3: Decoding.** Alice uses Bob's syndrome bits, her sub-block, Q , and \mathbf{H} as inputs to her LDPC decoder to correct all the discrepancies between Alice and Bob's sub-block. The LDPC decoder used is a serial-scheduled belief propagation decoder [35] implemented in C++.
- **Step 4: Reorganising.** After all the sub-blocks are reconciled, Alice reorganises all her sub-blocks into a single bit string (the reconciled key), \hat{K}_A , again of length n (similarly Bob to get \hat{K}_B).

Alice and Bob then proceed to privacy amplification to generate two identical and secure keys for cryptography purposes. Let us define the ratio, $r = s_{\text{final}}/n$, where s_{final} is the final key length required to achieve a set security level. To determine r we consider the security analysis in the finite-key length regime in [36–38]. Let us further define *ε-security* as the total failure probability, $ε$, of the protocol. Specifically, $ε = \tilde{ε} + ε_{\text{PA}} + ε_{\text{EC}} + ε_{\text{PE}}$, where $\tilde{ε}$ is the smoothing parameter for the smooth min-entropy calculation, $ε_{\text{PA}}$ is the failure probability of privacy amplification, and $ε_{\text{EC}}$ is the failure probability of error correction. The probability $ε_{\text{PE}}$ is somewhat more involved [36, 37, 39]. Consider the key, K_B^N , held by Bob (similar to K_B but including the m states that are to be sacrificed, i.e., $N = n + m$), and the key, E^N , held by the eavesdropper. Defining the combined quantum state held by Bob and the eavesdropper as $ρ_{K_B^N E^N} = (σ_K)^{\otimes N}$, where K and E represent individual components of K_B^N and E^N , respectively, then $σ$ is contained in the set $Γ_ξ$ defined by $\{σ : \|λ_m - λ_∞(σ)\| \leq ξ\}$, except with probability $ε_{\text{PE}}$. Here, $λ_m$ are the statistics derived from measurements on m samples of $σ$; $λ_∞(σ)$ is the probability distribution defined by the measurements on $σ$; and $ξ = \frac{1}{2} \sqrt{\frac{2 \log_2(\frac{1}{ε_{\text{PE}}}) + d \log_2(m+1)}{m}}$, where $d = 2$ is set due to the positive operator valued measure with 2 outcomes. These expressions are used to form an upper limit, Q^u , to Q that is used in determining the final key length. In many QKD variants this takes the simple form $Q^u = Q + ξ$. In more simpler terms, we can set an upper limit to what we think the true QBER, \hat{Q} , is and then determine the probability that this upper bound does not encompass \hat{Q} . For our protocol implementation, we use a similar analysis to [37] but with equal probability for each basis usage. Parameter estimation from individual bases was investigated, but in our experiments the QBER from each basis was found to be the same.

All of the above discussion leads us to a relation for r given by

$$r = \frac{s_{\text{final}}}{n} = A \left(1 - h \left(\frac{Q^u}{A} \right) - (1 - R_c) - Δ(n) \right), \quad (\text{A1})$$

where $A = \frac{p_{\text{det}} - P_m}{p_{\text{det}}}$, is the correction term due to the multi-photon emission at the single-photon source. In this latter relation, p_{det} is the probability of detecting at least one photon, P_m is the probability of multi-photon emission at the source. In Eq. (A1), $h(x) = -x \log_2 x - (1 - x) \log_2(1 - x)$ is the binary entropy function, and $Δ(n)$ is an additional penalty term given by

$$Δ(n) = \frac{7n \sqrt{\frac{1}{n} \log_2 \frac{2}{\tilde{ε}}} + 2 \log_2 \frac{1}{ε_{\text{PA}}} + \log_2 \frac{2}{ε_{\text{EC}}}}{n}. \quad (\text{A2})$$

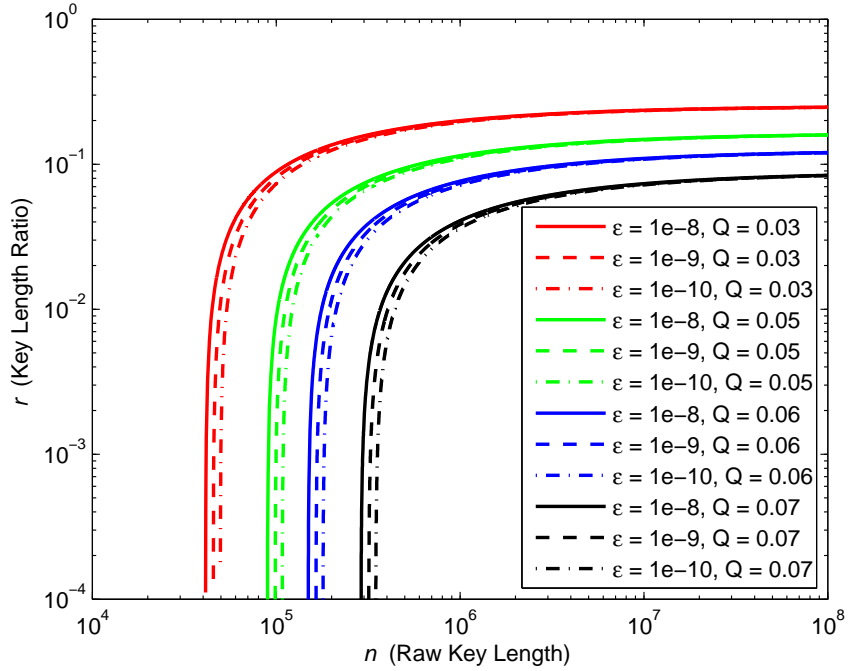


Figure 5 The ratio of key lengths, r , vs. the raw key length, n , for different security levels and different Q values. Here, the number of bits used for parameter estimation, m , is set at $m = n$.

We use the term $(1 - R_c)$ to compute the fraction of information leakage during reconciliation instead of the commonly used term $f_E h(Q)$, where f_E is the reconciliation efficiency. Noting that only the syndrome bits are disclosed during reconciliation, this efficiency can be written [40] $f_E = \frac{s_B}{nh(Q)} = \frac{1-R_c}{h(Q)}$, since $\frac{n-s_B}{n} = R_c$ holds for a given LDPC matrix.

In the main text we investigated the achievable r with respect to $\varepsilon = 10^{-10}$ with the results reflected in the main text. In all our reported secret key rates, we have set $m = n = 10^6$ to ensure a non-zero secret key rate at our required security level.

We note that our achievable r is a lower bound and can be further improved by optimising some of the parameters (e.g., $\tilde{\varepsilon}$) under defined constraints on the probabilities. Such optimisation was not carried out in our results. We have fixed $\tilde{\varepsilon} = \varepsilon_{\text{PA}} = \varepsilon_{\text{EC}} = \varepsilon_{\text{PE}} = \frac{\varepsilon}{4}$ and adopted $p_{\text{det}} = 0.6$, $P_m = 0.07$. Recent work [41, 42] on the second-order correlation function, $g^{(2)}(\tau)$ shows that (as a consequence of unknown vacuum contributions) the probability of obtaining a single photon is, in principle, unrelated to $g^{(2)}(0)$. That is, in any state-of-the-art implementation of single-photon QKD, $g^{(2)}(0)$ cannot be used directly as a measure of P_m . However, as described in 41, additional measurements to determine P_m directly negate this concern (at the cost of adjusting the secure key rate down for larger P_m). The value adopted above, $P_m = 0.07$, is based on measurements of our SIL-integrated SPPs. Typical examples of r as a function of n are shown in Fig. 5.

We close by outlining how our privacy amplification is actually implemented.

- **Step 1: Calculating r .** Alice uses Eqs. A1 and A2 to obtain r based on Q , ε , $\tilde{\varepsilon}$, ε_{PA} , ε_{EC} , ε_{PE} , n and m .
- **Step 2: Creating the hash function.** Following the procedure described in Section II.E of [43], Alice creates a Toeplitz matrix, \mathbf{T} , with n columns and $\lfloor rn \rfloor$ rows, where $\lfloor \cdot \rfloor$ is the floor operation. Alice sends \mathbf{T} to Bob.
- **Step 3: Secure hashing.** Alice and Bob apply \mathbf{T} to \hat{K}_A and K_B , respectively, and obtain two identical and secure key strings for cryptography purposes. [At some points, an *a priori* secret key will be consumed by Alice and Bob for authentication before the use of any key to encrypt/decrypt classical messages - we assume that such authentication is completed successfully.] A final check (hash) is taken on some small part of the keys to check the keys are identical - if they are not the protocol is aborted.

[1] E. Diamanti, H.-K. Lo, B. Qi, and Z. Yuan, Practical challenges in quantum key distribution, *npj Quantum Information* **2**, 1 (2016).

[2] F. Xu, X. Ma, Q. Zhang, H.-K. Lo, and J.-W. Pan, Secure quantum key distribution with realistic devices, *Reviews of Modern Physics* **92**, 025002 (2020).

[3] D. A. Vajner, L. Rickert, T. Gao, K. Kaymazlar, and T. Heindel, Quantum communication using semiconductor quantum dots, *Advanced Quantum Technologies* **5**, 2100116 (2022).

[4] V. Scarani, H. Bechmann-Pasquinucci, N. J. Cerf, M. Dušek, N. Lütkenhaus, and M. Peev, The security of practical quantum key distribution, *Reviews of Modern Physics* **81**, 1301 (2009).

[5] C. H. Bennett and G. Brassard, Quantum cryptography: Public key distribution and coin tossing, *Theoretical Computer Science* **560**, 7–11 (2014).

[6] F. Basso Basset, M. Valeri, E. Roccia, V. Muredda, D. Poderini, J. Neuwirth, N. Spagnolo, M. B. Rota, G. Carvacho, F. Sciarrino, and R. Trotta, Quantum key distribution with entangled photons generated on demand by a quantum dot, *Science Advances* **7**, eabe6379 (2021).

[7] F. Basso Basset, M. Valeri, J. Neuwirth, E. Polino, M. B. Rota, D. Poderini, C. Pardo, G. Rodari, E. Roccia, S. Covre da Silva, G. Ronco, N. Spagnolo, A. Rastelli, G. Carvacho, F. Sciarrino, and R. Trotta, Daylight entanglement-based quantum key distribution with a quantum dot source, *Quantum Science and Technology* **8**, 025002 (2022).

[8] J. Yin, Y.-H. Li, S.-K. Liao, M. Yang, Y. Cao, L. Zhang, J.-G. Ren, W.-Q. Cai, W.-Y. Liu, S.-L. Li, *et al.*, Entanglement-based secure quantum cryptography over 1,120 kilometres, *Nature* **582**, 501 (2020).

[9] H.-K. Lo, M. Curty, and B. Qi, Measurement-device-independent quantum key distribution, *Physical Review Letters* **108**, 130503 (2012).

[10] M. Bashar, M. Chowdhury, R. Islam, M. Rahman, and S. Das, A review and prospects of quantum teleportation, in *2009 International Conference on Computer and Automation Engineering* (IEEE, 2009) pp. 213–217.

[11] S.-K. Liao, W.-Q. Cai, W.-Y. Liu, L. Zhang, Y. Li, J.-G. Ren, J. Yin, Q. Shen, Y. Cao, Z.-P. Li, *et al.*, Satellite-to-ground quantum key distribution, *Nature* **549**, 43 (2017).

[12] X. Ma and H.-K. Lo, Quantum key distribution with triggering parametric down-conversion sources, *New Journal of Physics* **10**, 073018 (2008).

[13] T. Kupko, M. von Helversen, L. Rickert, J.-H. Schulze, A. Strittmatter, M. Gschrey, S. Rodt, S. Reitzenstein, and T. Heindel, Tools for the performance optimization of single-photon quantum key distribution, *npj Quantum Information* **6**, 29 (2020).

[14] H.-K. Lo, X. Ma, and K. Chen, Decoy state quantum key distribution, *Phys. Rev. Lett.* **94**, 230504 (2005).

[15] P. Senellart, G. Solomon, and A. White, High-performance semiconductor quantum-dot single-photon sources, *Nature Nanotechnology* **12**, 1026 (2017).

[16] I. Aharonovich, D. Englund, and M. Toth, Solid-state single-photon emitters, *Nature Photonics* **10**, 631 (2016).

[17] T. Heindel, C. A. Kessler, M. Rau, C. Schneider, M. Fürst, F. Hargart, W.-M. Schulz, M. Eichfelder, R. Roßbach, S. Nauerth, *et al.*, Quantum key distribution using quantum dot single-photon emitting diodes in the red and near infrared spectral range, *New Journal of Physics* **14**, 083001 (2012).

[18] K. Takemoto, Y. Nambu, T. Miyazawa, Y. Sakuma, T. Yamamoto, S. Yorozu, and Y. Arakawa, Quantum key distribution over 120 km using ultrahigh purity single-photon source and superconducting single-photon detectors, *Scientific Reports* **5**, 14383 (2015).

[19] Ç. Samaner, S. Paçal, G. Mutlu, K. Uyanık, and S. Ateş, Free-space quantum key distribution with single photons from defects in hexagonal boron nitride, *Advanced Quantum Technologies* **5**, 2200059 (2022).

[20] M. Leifgen, T. Schröder, F. Gädke, R. Riemann, V. Métillon, E. Neu, C. Hepp, C. Arend, C. Becher, K. Lauritsen, *et al.*, Evaluation of nitrogen-and silicon-vacancy defect centres as single photon sources in quantum key distribution, *New Journal of Physics* **16**, 023021 (2014).

[21] N. L. Piparo, M. Razavi, and W. J. Munro, Measurement-device-independent quantum key distribution with nitrogen vacancy centers in diamond, *Physical Review A* **95**, 022338 (2017).

[22] T. Gao, M. von Helversen, C. Anton-Solanis, C. Schneider, and T. Heindel, Atomically-thin single-photon sources for quantum communication, *npj 2D Materials and Applications* **7**, 4 (2023).

[23] I. Aharonovich, J.-P. Tetienne, and M. Toth, Quantum emitters in hexagonal boron nitride, *Nano Letters* **22**, 9227 (2022).

[24] H. Z. J. Zeng, M. A. P. Ngyuen, X. Ai, A. Bennet, A. S. Solnstev, A. Laucht, A. Al-Juboori, M. Toth, R. P. Milidren, R. Malaney, *et al.*, Integrated room temperature single-photon source for quantum key distribution, *Optics Letters* **47**, 1673 (2022).

[25] X.-W. Chen, S. Götzinger, and V. Sandoghdar, 99% efficiency in collecting photons from a single emitter, *Opt. Lett.* **36**, 3545 (2011).

[26] L. Sortino, P. G. Zotev, C. L. Phillips, A. J. Brash, J. Cambiasso, E. Marensi, A. M. Fox, S. A. Maier, R. Sapienza, and A. I. Tartakovskii, Bright single photon emitters with enhanced quantum efficiency in a two-dimensional semiconductor coupled with dielectric nano-antennas, *Nature Communications* **12**, 6063 (2021).

[27] T. Gao, L. Rickert, F. Urban, J. Große, N. Srocka, S. Rodt, A. Musial, K. Źołnacz, P. Mergo, K. Dybka, *et al.*, A quantum key distribution testbed using a plug&play telecom-wavelength single-photon source, *Applied Physics Reviews* **9**, 011412 (2022).

[28] M. Rau, T. Heindel, S. Unsleber, T. Braun, J. Fischer, S. Frick, S. Nauerth, C. Schneider, G. Vest, S. Reitzenstein, *et al.*, Free space quantum key distribution over 500 meters using electrically driven quantum dot single-photon sources—a proof of principle experiment, *New Journal of Physics* **16**, 043003 (2014).

[29] P. Grünwald, Effective second-order correlation function and single-photon detection, *New Journal of Physics* **21**, 093003 (2019).

[30] J. R. Chavez-Mackay, P. Grünwald, and B. M. Rodríguez-Lara, Estimating the single-photon projection of low-intensity light sources, *Physical Review A* **101**, 053815 (2020).

[31] Y. Guo, C. Gao, D. Jiang, and L. Chen, 100 Mbps Reconciliation for Quantum Key Distribution Using a Single Graphics Processing Unit, *SN Computer Science* **2**, 1 (2021).

[32] T. J. Richardson, M. A. Shokrollahi, and R. L. Urbanke, Design of Capacity-Approaching Irregular Low-Density Parity-Check Codes, *IEEE Transactions on Information Theory* **47**, 619 (2001).

[33] D. Elkouss, A. Leverrier, R. Alléaume, and J. J. Boutros, Efficient Reconciliation Protocol for Discrete-Variable Quantum Key Distribution, in *Proceedings of IEEE International Symposium on Information Theory* (IEEE, 2009) pp. 1879–1883.

[34] X.-Y. Hu, E. Eleftheriou, and D.-M. Arnold, Regular and Irregular Progressive Edge Growth Tanner Graphs, *IEEE Transactions on Information Theory* **51**, 386 (2005).

[35] E. Sharon, S. Litsyn, and J. Goldberger, Efficient Serial Message-Passing Schedules for LDPC Decoding, *IEEE Transactions on Information Theory* **53**, 4076 (2007).

[36] V. Scarani and R. Renner, Quantum cryptography with finite resources: Unconditional security bound for discrete-variable protocols with one-way postprocessing, *Physical Review Letters* **100**, 200501 (2008).

[37] R. Y. Cai and V. Scarani, Finite-key analysis for practical implementations of quantum key distribution, *New Journal of Physics* **11**, 045024 (2009).

[38] P. Chaiwongkhot, S. Hosseini, A. Ahmadi, B. L. Higgins, D. Dalacu, P. J. Poole, R. L. Williams, M. E. Reimer, and T. Jennewein, Enhancing Secure Key Rates of Satellite QKD Using a Quantum Dot Single-Photon Source, arXiv preprint arXiv:2009.11818 [10.48550/arXiv.2009.11818](https://arxiv.org/abs/2009.11818) (2020).

[39] D. Bunandar, L. C. G. Govia, H. Krovi, and D. Englund, Numerical finite-key analysis of quantum key distribution, *npj Quantum Information* **6**, 104 (2020).

[40] D. Elkouss, J. Martinez-Mateo, and V. Martin, Information reconciliation for quantum key distribution, *Quantum Information and Computation* **11**, 0226 (2011).

[41] P. Grünwald, Effective second-order correlation function and single-photon detection, *New Journal of Physics* **21**, 093003 (2019).

[42] J. R. Chavez-Mackay, P. Grünwald, and B. M. Rodríguez-Lara, Estimating the single-photon projection of low-intensity light sources, *Phys. Rev. A* **101**, 053815 (2020).

[43] J.-P. Bourgoin, N. Gigov, B. L. Higgins, Z. Yan, E. Meyer-Scott, A. K. Khandani, N. Lütkenhaus, and T. Jennewein, Experimental Quantum Key Distribution With Simulated Ground-to-Satellite Photon Losses and Processing Limitations, *Physical Review A* **92**, 10.1103/PhysRevA.92.052339 (2015).